University of Groningen

Master Thesis

Charge collecting microscopy of *in-situ* switchable phase-change memory cells

Author:
R.W. Schuitema

Supervisor:
Ir. J. L. M. Oosthoek

Group Leader:
Prof. dr. Ir. B.J. Kooi

February 22, 2011

Abstract

This reports presents the results from charge collecting microscopy (CCM) study performed on Phase-change memory (PCM). CC uses the electron beam of the Scanning Electron Microscope (SEM) to inject charge carriers into the sample and measure the currents by a picoammeter called the EBIC amplifier or specimen current (SC) detector. To do so, a home built probe station was manufactured which allows the PCM cell to be switched *in-situ* in the SEM. Because of difficulties in obtaining high quality images, several ways of enhancing were proposed. The best results are gained with reducing the thickness of the passivation by either Focussed Ion Beam (FIB) milling or etching with Buffered Hydrofluoric acid. The resulting images did not have enough detail to precisely observe the amorphous mark but did reveal the location of it. Therefore the Thomson effect previously reported in PRAM cells could be observed *in-situ*.

Contents

Chapter 1

Introduction

Our rapidly growing demand of data storage drives the semiconductor industry to constantly search for a better memory device. One of most commercially used memory devices today is Flash. Flash memories are non-volatile, which means no power is needed to maintain the information on the device. However flash has a lot of limitations. The long relative long programming time, in the order of microseconds, only allows writing information in large blocks. Flash has a finite number of program-erase cycles (P/E cycles) typically in the order of 100 000. Furthermore, due to high programming voltages (exceeding 10 V), flash consumes a lot of energy and, maybe more important, it is projected that further downscaling will be increasingly difficult in the near future.

A new possible candidate is the Phase Change Memory (PCM) or PRAM. Phase-Change memory uses a rapid, reversible, thermally-induced transformation between the substantially atomically ordered and atomically disordered phases of certain, semiconductors to store information in a non-volatile fashion [1]. The simple geometry of the cell makes it easy to scale it down. The number of P/E cycles have been reported to be more than 100 000 000 times. Although prototype applications using PRAM already exist, fundamental problems such as retention and production yield still need to be overcome, in order to achieve a commercial breakthrough.

To investigate these cells, which have a typical dimension of a few hundred nanometer, the Transmission Electron Microscope (TEM) is often used. One of the drawbacks of using the TEM is the laborious sample preparation. This study

investigates if the Scanning Electron Microscope (SEM) could be used to provide an easy way of examining these PRAM cells. This is done by Charge Collecting Microscopy (CCM). This technique uses the electron beam of the SEM to inject charge carries in the sample and measure the currents by a picoammeter, called the specimen current (SC) detector .

Chapter 2

Samples and techniques

2.1 Phase change memory cell

Phase change materials are already widely used in optical data storage applications. The phase change materials are characterized by two different phases, a crystalline phase and an amorphous phase. In optical devices a laser beam locally melts the background and then is rapidly quenched [2]. This creates amorphous spots which have a lower reflection than the crystalline surrounding. This reflection contrast is used in reading the information in a binary matter. Re-writing occurs by heating the spot just above the glass-transition temperature. The mobility of the atoms increases due to this added energy which allows them to rearrange into a energetically more favorable crystalline structure.

Not only the optical, but also the electrical properties between the two states are very distinctive. The resistivity between the crystalline and the amorphous state differ about three orders of magnitude, which is even bigger than the optical contrast. Therefore using the electrical properties of phase change materials for data storage is very promising. The PCM consist of a piece of phase-change material connected in between two electrodes. Switching can be established by high-frequency pulses.

If the cell is in the (initial) low resistance crystalline state (binary 1), it can be switched into the higher resistance amorphous state (binary 0) by applying a voltage pulse (RESET pulse) on the material [3]. This pulse has to be of such a magnitude that by Joule-heating the temperature of the material is reaching the

melting point at the part where the current density is the highest. The locally molten spot is rapidly quenched, leaving the atomic structure in a disordered state. This region, referred to as the amorphous mark, is creating a barrier for conduction electrons and thus increasing the resistance of the cell. To switch the cell back to the lower resistance crystalline state a voltage pulse (SET pulse) which is longer and has a lower voltage than RESET pulse is applied. The pulse adds enough energy to the cell that by Joule-heating the cell reaches the crystallization temperature. The amorphous mark is crystallized again lowering the resistance. Figure 2.1 is showing the switching between two states in the PCM.

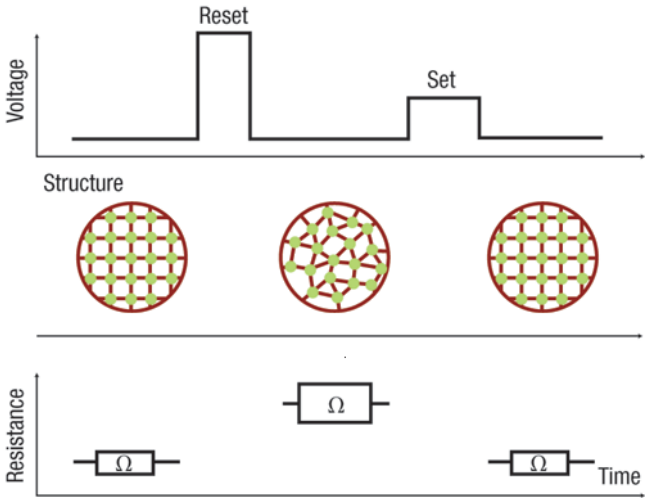

Figure 2.1: *switching of the phase change memory cell is done by a set and a reset pulse [3].*

2.1.1 Geometry

The cells used in the experiments are test cells produces by NXP semiconductors, called "dog bone cells". Figure 2.2 shows a non scaled schematic drawing of such a cell. Coppers electronic connectors called "runners" provide the connection from the phase-change material to two aluminum bonding pads.

A lot of processing steps are involved in manufacturing these cells. First a stack of SiO_2, SiC, and Si_3N_4 layers is deposited on a silicon wafer. Then copper is evaporated on top of this and by lithography the runner pattern is made. Next

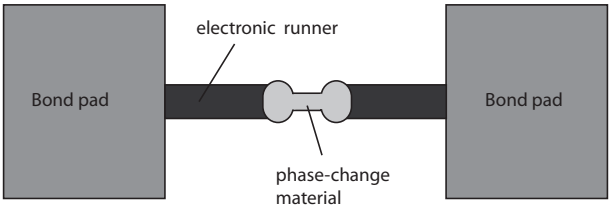

Figure 2.2: *Schematic drawing of a phase-change memory cell (not on scale).*

a blanket layer of phase-change material was deposited over these runners. A, to etchant non-reactive, hard mask, patterned in the shape of the cell, is deposited on top of this. After that an etchant is used to etch phase-change material away, the typical dog-bone shape is left behind lying over the runners resembling bridge. Again, a stack of SiO_2, SiC, and Si_3N_4 layers were deposited on top of the phase-change material, protecting the cell. Then the electrical throughputs were processed on top of that providing the the connection between the bond pads and the runners. The complete geometry is depicted in Figure 2.3.

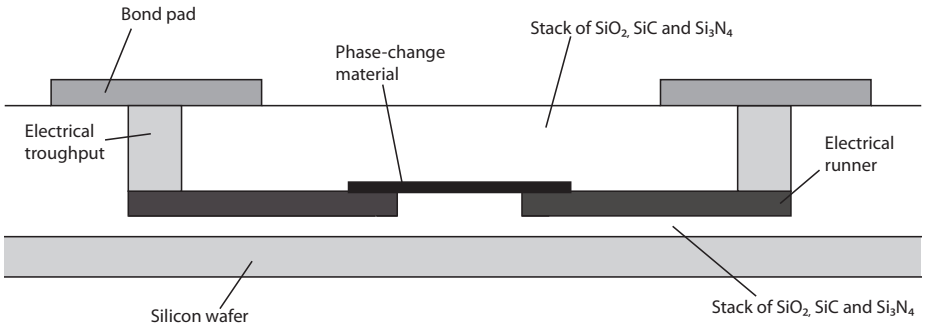

Figure 2.3: *Geometry of the memory cell*

2.2 Charge Collection Microscopy

Charge-collection Microscopy (CCM) and specifically electron beam-induced current (EBIC) is often used in examining semiconductor devices. It is a simple method to obtain information about p-n junctions as well as grain boundaries in semiconductor materials [4]. The high energy beam of the scanning electron

microscope (SEM) is used to create electron-hole pairs (EHPs) in the specimen due to excitation of the valence electrons into the conduction band. A single primary electron can produce 10.000 EHPs. If the (semiconductor) specimen has an internal field as will be present in p-n junctions or Schottky barriers, and the electron beam strikes the specimen in or near the depletion region, the electrons and holes will get separated due to this electrical field. If a picoammeter is connected to the contacts of the sample, a current I_{ebic}, will flow which can measured. Because of charge multiplication, the magnitude of this current is much higher than that of the electron beam. The position of the electron beam is coupled to the input of the picoammeter so a image is build up resulting in EBIC imaging. A schematic representation of this measurement technique is depicted in Figure 2.4

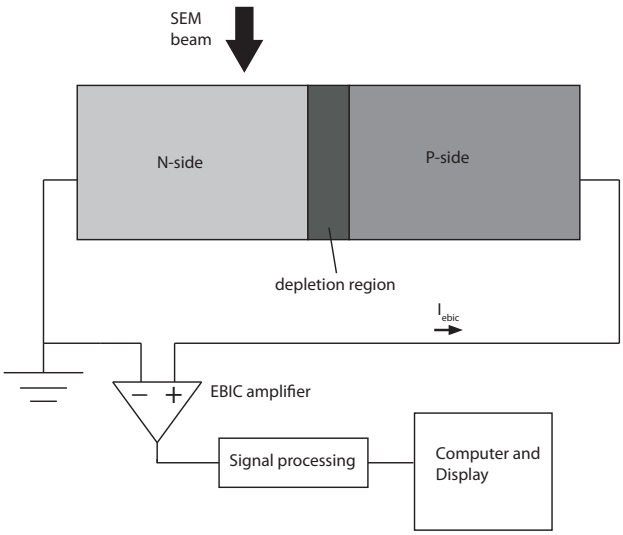

Figure 2.4: *Schematic drawing of the setup for examination with EBIC, with a p-n junction connected to the SC detector.*

Because of the relatively high beam energies required to preform EBIC, typically in the order of 10-20 keV, it is limited in the evaluation of Metal-Oxide-Semiconductor (MOS technology); The gate oxide sensitivity to the primary electron beam causes failure of the transistors at high acceleration voltages. Therefore another method of charge-collection microscopy called resistive contrast imaging (RCI), which actually is a modified EBIC method, was developed

for measuring the internal resistance in a non-destructive manner [6]. The current is sampled with the normal EBIC instrumentation, but the difference is that RCI is using lower beam energies and will thus not create EHPs. In RCI one solely measures the current between two test nodes, so that it can image open en shorted connections. Because the same setup is used for both EBIC and RCI the difference between the two methods lie in energies of the electron beam and the samples of interest. In the case of RCI only a part of the electrons of the electron beam are measured, resulting in a current lower than the electron beam (and therefore orders of magnitude lower than a measured EBIC signal). The setup for the RCI method is schematically drawn in Figure 2.5

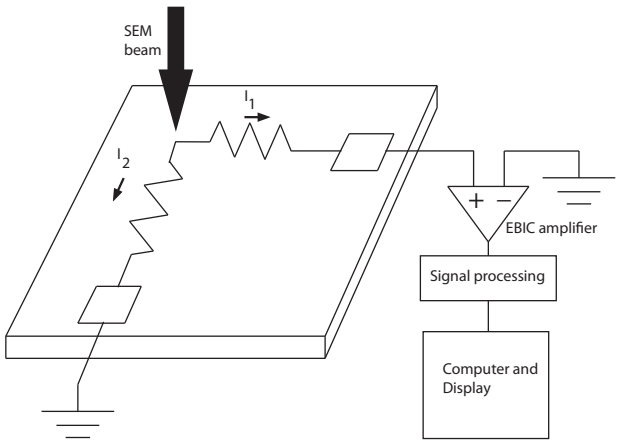

Figure 2.5: *Schematic drawing of the RCI setup. This is basically the same as the EBIC setup, with the only difference that a lower voltage electron beam is used.*

To get a little bit of experience with the EBIC method, it was first tested on a regular p-n junction diode. The diode was connected as depicted in Figure 2.4. A Philips XL 30 SEM was used with a Phillips SC detector. The relative slow response of this detector does not allow operation in TV scanning mode. A slower scan mode has to be used in order to get a stable signal. This reduces the flexibility to navigate the electron beam to designated locations.

Figure 2.6 shows the SE image (a) and the EBIC image (b) of the diode. On the SE image the metal contacts of the diode are visible, but it contains no information about the location of the underlying depletion region. The EBIC

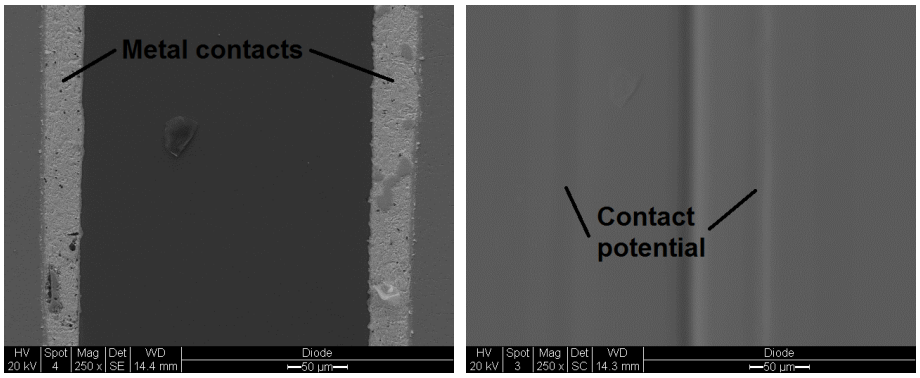

(a) (b)

Figure 2.6: *(a) SE image of a diode. (b) EBIC image of the same diode, clearly showing the depletion region in the middle.*

Figure 2.6b, does reveal this. The black line in the middle of Figure 2.6b indicates an electric field therefore showing the interface between the n-type and the p-type material. Though a bit less clear, two more lines are visible on the image. these indicate an interface of materials as well. At the interface of the two differ materials a small electrical field is present by Fermi level equilibration, called the contact potential. This field is far weaker than the depletion region of the two doped materials thus creating a less distinctive EBIC signal.

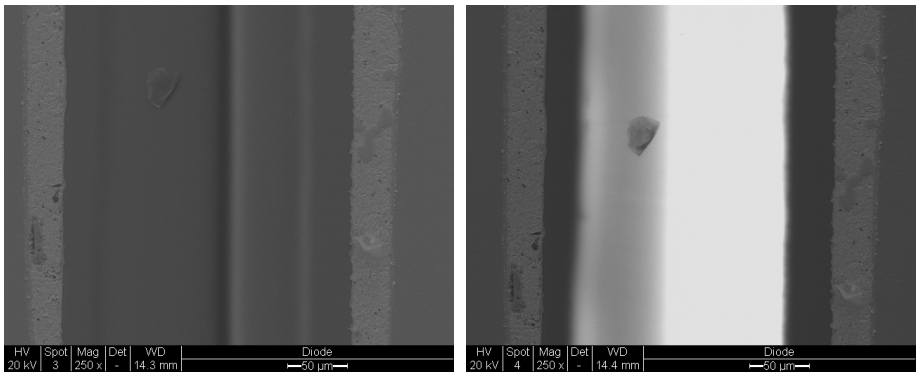

(a) (b)

Figure 2.7: *(a) Mixed mode image of the diode. This option allows a combination of SE and EBIC mode. (b) Mixed mode image with reversed connection resulting in an inverted image for the EBIC mode*

Figure 2.7 shows the mixed mode option of the SEM. In this image the data of both the SE as the EBIC mode are collected (25% SE and 75% SC). 2.7 b shows the same sample but with a reversed connection. This results in an I_{ebic} with an opposite sign, therefore displaying the depletion region as white.

2.2.1 Charge Collecting Microscopy with Phase-change materials

A study in investigating phase-change materials with a specimen current detector has been preformed previously. The study, done by R. Pandian, involved making crystalline spots on an amorphous phase-change blanket layer with use of the atomic force microscope (AFM) [7]. The operation of the AFM is explained in more detail in the next chapter. $Ge_2Sb_{2+x}Te_5$ (GST) phase-change material was deposited on a Molybdenum electrode by magnetron DC sputtering. The high current density of the AFM tip was used to locally apply an electrical DC pulse in order to make the crystalline marks. The setup showed in Figure 2.8 was used to image the crystalline spots using the specimen current detector.

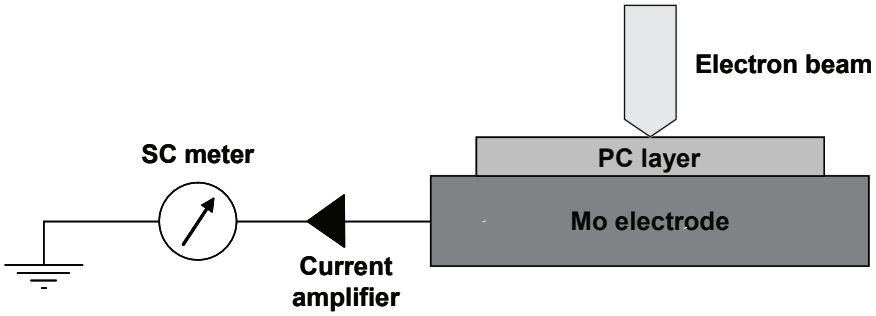

Figure 2.8: *Specimen current setup for imaging crystalline marks in Phase-change blanket layers*

Figure 4.8b shows the AFM written crystalline marks on the PC layer imaged in the SEM in the SE mode. It was shown that the spots have a diameter of about 50 nm. Figure 4.4c shows the same spots but now in RCI mode. A clear contrast is visible between crystalline marks and amorphous background. This

shows the possibility of using SC for imaging phase-change memory cell, though one has to keep in mind no passivation layer was used in these experiments and the geometry is completely different from the test cells used in this research.

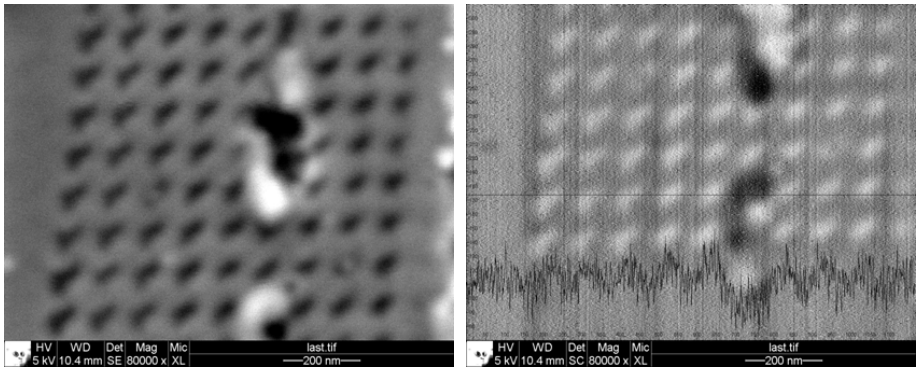

(a) (b)

Figure 2.9: *AFM written crystalline marks imaged with the SEM in SE and RCI mode*

Chapter 3

Experimental

Preforming CCM on the PCM cells did not directly result in the same high quality images as with the PN-diode. The contrast mechanism is completely different because of the complicated geometry and the unfamiliar properties of phase-change materials regarding EBIC and RCI. Different methods on the visualization of the PCM cells with CC microscopy were proposed. The next chapter describes most of the steps taken in our work to reach the goad of good quality CCM images of the PCM cells.

3.1 Connecting the cells

To make the electrical connections from the bond pads to the SC detector a chip carrier device was manufactured. This device contained two copper electronic contacts where two cables were attached to providing the connection to the SC detector. The PCM is connected to the copper contacts by ultrasonic wire bonding. The wire bond machine used, bonds aluminum wires with a diameter of 25 μm. Because the cell is very sensitive to static discharging, it is very important to wear a grounding strap. To decrease the risk of a high potential difference between the contacts a conductive jumper was attached to both contacts while bonding. This jumper could then be disconnected for the SC measurements. Figure 3.1 shows the bond wires attached to the bond pads. Two different methods of connecting to the cell were investigated. The first was connecting both sides of the cell to the SC detector. The second way was con-

necting one side of the cell to the ground and the other to the SC detector. In order to investigate the amorphous mark it was found that the second method was preferable as explained in the next chapter.

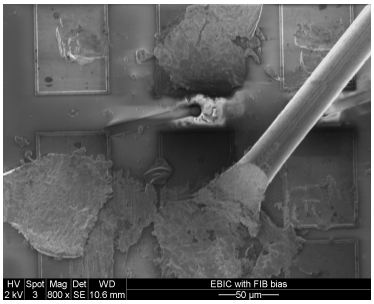

Figure 3.1: *Bonded wires attached to the bond pads*

3.2 Voltage biased grid

Because both contrast and resolution were not sufficient to create high quality images, several methods were investigated to enhance this. One was the electron shielding by a biased grid. It is assumed that the electrons would be far more mobile in the phase-change material than they would in the passivation layer. Therefore a small circular grid was mounted just above sample near the PCM, and a positive bias was applied by an external power supply. By positively biasing the grid electrons would be drawn towards it. Because of the higher conductance, a relative smaller part of the electrons would be drawn out of the phase-change material than out of the passivation layer. The small ring did not seemed to have a great effect, so a big conductive plate was used as a grid to create a large surface. The power supply created a lot of noise, probably due to an unstable signal. A home built stabilizer box with a 7812 voltage regulator and some capacitors to filter out high frequent signals did reduced the noise but did not enhanced the contrast.

3.3 Conductive organic layer PEDOT:PSS

To reduce the charging effects of the samples to be imaged with the electron beam in the SEM an organic conductive polymer layer was spin coated

onto the samples. The material used was a Poly(3,4-ethylenedioxythiophene) poly(styrenesulfonate),or PEDOT:PSS. The big advantage of PEDOT:PSS is it dissolves in water, thus the layer can easily be removed if necessary. The layer was put on the samples using a spin coater. Spin coating is a technique which allows deposition of very thin films on a solid substrate. The spin coater is a device which allows fast rotation of a sample and by an adjustable program the rotations per minute and the duration of spinning can be set. By putting a droplet of the in water dissolved PEDOT:PSS on the sample and spin it, due to the centrifugal forces the droplet smears out over the surfaces creating a thin film. While spinning the samples is kept in place by a vacuum chuck. The spin coater was programmed to spin 10 seconds with 500 rpm and 240 seconds with 2500 rpm.

3.4 Focussed Ion Beam

When an electron beam hits the sample it begins to broaden due to elastic scattering effects. The result is the well known pear-shaped interaction volume. This results in the fact the resolution of the image is not the theoretical resolution of the microscope, known as the lateral resolution. Therefore a the area of interest should not be to deep into the sample as this reduces the contrast. In the case of the PCM cells the electrons have to penetrate through a thick passivation layer. To enhance the contrast a method was necessary to partly remove this layer, in such a way the cell was still functional. One of the methods was the Focused Ion Beam (FIB) to ablate a part of the passivation layer above the cell. The FIB resembles a SEM however, instead of emitting high energy electrons to scan a sample the FIB is based on a focused beam of ions (in this case Galium). Because the ions are far bigger and heavier than electrons, the beam could be used to ablate the material of specimen within a resolution in the order of 10nm. The specific FIB used (a Tescan Lyra 3 FEG) has both an electron and an ion source. This way samples can be imaged with either electrons or ions.

Figure 3.2 shows the devices after the FIB was used to remove the passivation layer. Figure 3.2 b shows a SE close up where one could clearly see the PCM lying under the removed area.

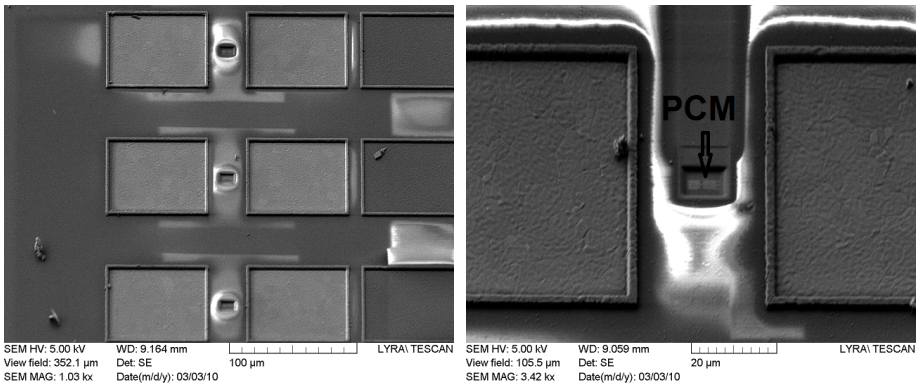

(a) (b)

Figure 3.2: *(a) SE image of three cells with a "hole" of removed SiO_2 done by the FIB. (b) Close up of a hole milled by the FIB.*

3.5 Atomic Force Microscope

The FIB does not allows accurate measurements on how much material is removed in the process. Therefore an AFM was used. These images can also provide a good insight of the surface morphology after the FIB treatment. The AFM is a high resolution scanning probe microscope. The AFM uses a cantilever with a very sharp tip which has a radius of curvature in the order of nanometers. When the tip slowly approaches the surface of the specimen the interacting forces between the tip and the surface causes the cantilever to deflect according to Hooke's law. This deflection is then measured with a laser beam spot reflecting on the end of the cantilever to an array of photo diodes. Figure 3.3 is showing a schematic setup of the AFM.

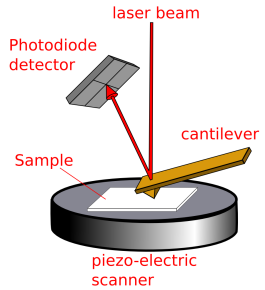

Figure 3.3: *Schematic representation of the setup of the AFM*

Figure 3.4a shows an AFM picture of the surface of the sample after removal of the passivation layer with the FIB. Half of the dog bone structure of the cell is visible on this picture in the area milled by the FIB. The reason the AFM measures the underlying structure of the phase-change material is shown in 3.4b. This displays the profile measurements of the AFM picture, indicated with the blue line in 3.4a. It is shown that during the FIB treatment a hole of 280 nm deep (in the z-direction) was created. Furthermore it shows that on top of the cell structure there is more material than in the in the rest of the milled hole. This is caused by the hard mask layer present on top of the memory cell which is about 80 nm thick.

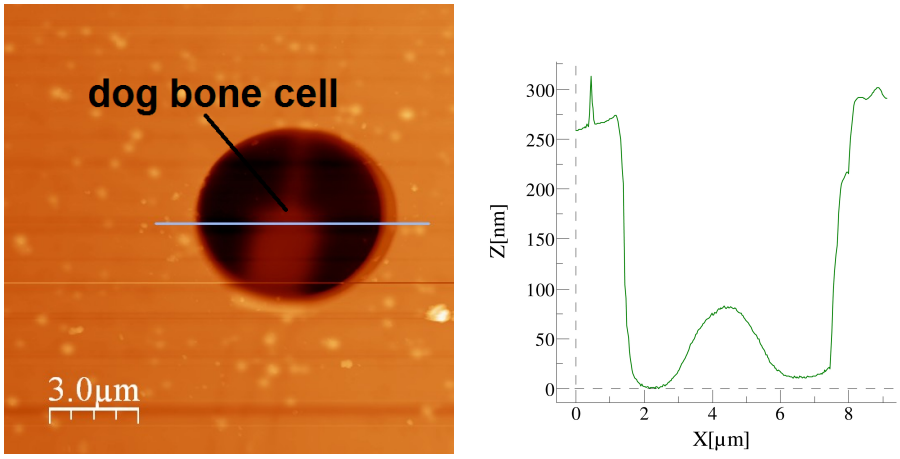

(a) (b)

Figure 3.4: *(a) AFM image of a hole made by the FIB. On the bottom of the hole an imprint of the phase-change cell is visible. (b) Profile of the hole taken over the blue line in (a).*

The height difference due to the hard mask layer present on the memory cell can be more clearly visualized with a 3-D projection of the same image (Figure 3.5). It shows the imprint of the runners to the cell in the region around the circular area removed by the FIB. In this area the imprint of the cell itself is highly visible.

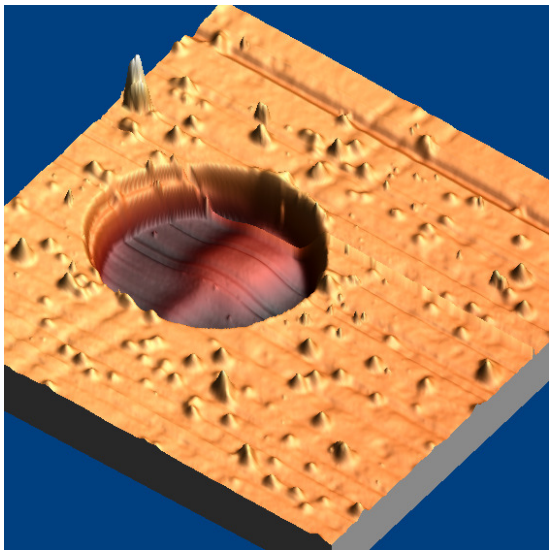

Figure 3.5: *A 3-D projection of the image in Figure 3.4 with the clear imprint of the hard mask at the bottom of the hole*

3.6 HF etching

Another method which was used to remove the passivation layer was by wet hydrofluoric acid (HF) etching. Hydrofluoric acid is a very corrosive acid widely used for its property to dissolve SiO_2 and Si_3N_4. The chemical reaction can be described by [8]

$$SiO_2 + 6HF \rightarrow H_2SiF_6 + 2H_2O \tag{3.1}$$

First a 40% HF solution was used. A droplet of the solution was placed on the sample. This solution has a very fast reaction time resulted in over etching and complete removal of the surrounding passivation layers of the phase-change memory cells. Some of the cells were even removed completely. Other cells were physically separated from the substrate because the passivation layer underneath the cell was etch away too. These cells are impossible to switch as they cannot release their energy after the applied pulse. Quenching is essential to stabilize the disordered atomic structure. Removal of the complete surrounding passivation layer causes the cell to be fragile and therefore most of these cells were broken.

To have more control over the speed of the reaction buffered hydrofluoric

acid (BHF) was used. This was preformed at the special facilities in the clean room of NanoNed. The samples were placed on a Teflon holder that was dipped into the solution. BHF consist of a mixture of concentrated HF and a buffering agent, in this case HN_4F. This buffering agent is raising the pH of the acid thereby lowering the etch rate. It also keeps the pH constant during the etching process. This results in a well-controlled etch rate. A wafer was broken into smaller pieces each containing a number of functional cells. Each piece of this batch was etched for a different period of time in order to find the maximum time that could be etched while still preserve an functional cell. When after the first etching session it was found that all the cells were still functional, etching was performed a second time on the cells which were initially etched for the shortest time to etch them even further. Table 3.1 shows how long the different samples are etched.

Sample name	Etch time in BHF 15% (min)	Etch time in BHF 10% (min)
E1	3	15
E2	6	15
E3	8	15
E4	10	-
E5	12	-
E6	16	-

Table 3.1: *Etching times of the samples in BHF 10% and BHF 15%*

The etching was preformed in two different clean rooms both unfortunately containing a different type of BHF solution. The first BHF solution used was a BHF 15% (where the 15% is referring to the concentration of the buffer agent) which has an etch rate of 50 nm/min for SiO_2 at 20°C. The second solution was BHF 10% which has an etch rate of 75 nm/min for SiO_2 at 20°C. The etching rates of SiC and Si_3N_4 are not known. Though the passivation layer is a stacking of SiO_2, SiC, and Si_3N_4 it is assumed that it mainly consist of SiO_2. Therefore taking into account the etching rates of the SiO_2 should give a rough estimate of the amount of passivation layer etched away by the BHF. Figure 3.6 shows the amount of passivation layer that is etched away for each sample if it purely consisted of SiO_2. None of the samples that were etched again in the BHF 10% were still functional. We can conclude that the optimum is lying

between 800 nm and 1200 nm. One has to realize that the layer on top of the PCM is still around 150 nm thicker than the surrounding area.

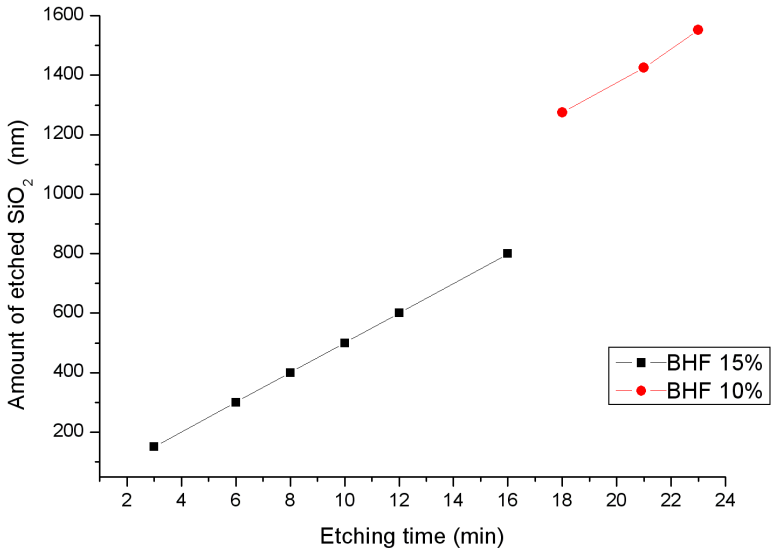

Figure 3.6: *This graph shows an estimation of the amount of SiO_2 that was etched away for every sample*

3.7 Probe station

For other studies the measurements on phase-change memory cells are performed on a home built probe station setup. This setup, schematically depicted in Figure 3.7, consist of a pulse generator providing the SET and RESET pulses, an oscilloscope to examine the incoming and outgoing pulses and a source meter to measure the resistance before and after switching the cell. The 3.2kΩ series resistance is necessary for certain geometry of the cell to supply the right potential over the cell. This series resistance has to be very close to the cell in order to make capacitive currents related to the stray capacitance as small as possible. The electrical connection made to the cell is provided with two probe needles.

With the wire bonding technique it was only possible to bond one cell at a

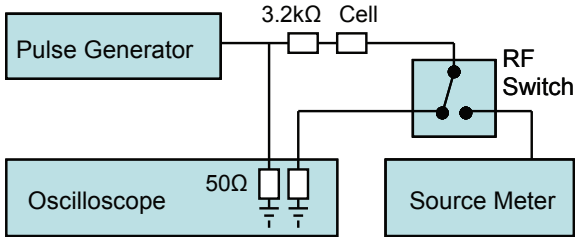

Figure 3.7: *Schematic drawing of the setup used to measure the phase-change cells, made by Jasper.*

time. Due to the fact a cell was easily damaged by electrical pulses or the wire bonds broke from the bond pads, it was a time consuming part of the experiment. Also the versatility of this method is far from good, as for example it does not allows a quick switch from connecting one side of the cell to the ground and the other side to the SC detector to reversing this connection. These complications could be overcome by using the probe station for the RCI measurements in the SEM, but as it is far to big to be placed in the SEM, a special mini probe station was designed. This mini probe station was constructed by the workshop. It allows the cell to be probed outside of the SEM and after that the mini probe station can be mounted on the stage of the SEM. The probe station had to have the same connections as the regular probe station to make it possible to measure the resistance and switch the cell, all while the cell is in the SEM. The connections were made by a vacuum throughput. The probe station also had to contain several relay switches in order to switch the ground and RCI signal and to switch the series resistance on and off, again we want this series resistance to be as close to the needles as possible to reduce the energy of the capacitive pulses.

3.7.1 Probe needles

The first challenge consists of making the probe needles. The probe needles used in the probe station of the measurement setup outside the SEM were commercially needles mounted on a holder containing several series resistances. This holder was far to big to fit in the SEM therefore a method was invented to make the needles ourself. Two tungsten tips (Picoprobe) with a shaft diameter

of 0.51 mm and a tip radios of <5.0 microns were used. The tips are nickel plated allowing the shaft of the tips to be soldered. To make the probing needles both of the tips were manually placed on the bond pad of either side of a cell by using preparation light microscope. The bond pads are of a distance of 40 μm apart, so when placing the tips in the center of the bond pads, the distance was about 120 μm. The needles were lined up in the right position on a piece of double-sided tape, after which a drop of two components epoxy glue was applied to them. It was found that the epoxy glue does not stick to the smooth surface of sticker paper, so this was placed underneath the glue. This is depicted in Figure 3.8. After 24 hours of hardening, the needles were gently removed from the surface. After that they were mounted on a small print board by soldering.

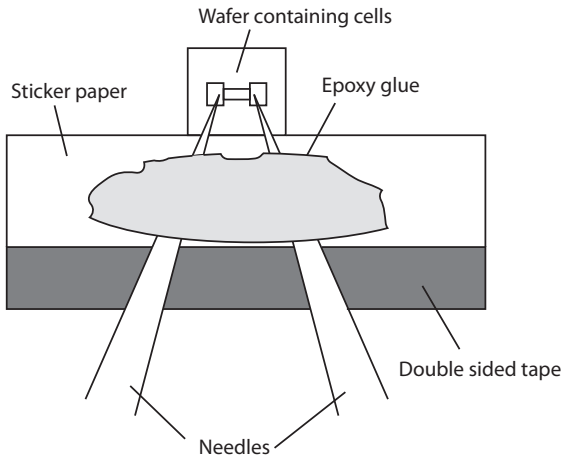

Figure 3.8: *Schematic drawing of way the home built probe needles were made.*

3.7.2 Mini-probestation hardware

For positioning the needles were mounted on small a XYZ manipulator. When the glue was applied and the needles were installed at the print board it was hard to accomplish both the needles were exactly at the same height. This is even a known problem with the commercially Multi-Z probes used in the probe station of the regular setup. Therefore a mounting was placed allowing to rotate the needles in the YZ-plane, enabling to compensate the difference in height between the two needles. A sample holder was placed on a manipulator

in the Y-direction, it also had a lift function to move the sample up and down for about 2 mm. This way the contact with the cell could be broken without using the XYZ-manipulator. The result of the probe station can be seen on Figure 3.9. The figure also features the sub-D connector establishing all the connections which are explained below.

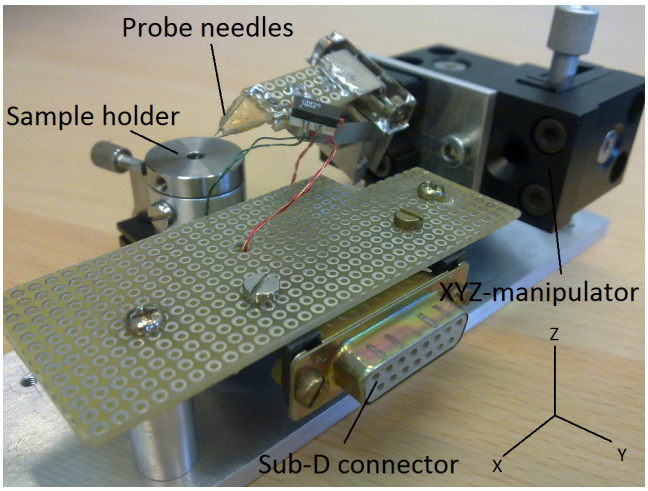

Figure 3.9: *The home built mini-probestation used for in-stitu SEM measurements*

3.7.3 Electrical circuit of the mini-probe station

To make the connection with the probe station a sub-D connector was chosen. Though these connector are not designed for high frequency pulses it has the advantage that it is quick and easy to establish the connection. The vacuum throughput is equipped with seven SMB connectors, so custom cables were made with the sub-D connector on one side and SMB connectors to the other side. Three coaxial cables were used to make the connection with the measurement setup for pulses to and from the cell and reading the resistance. For the switching of the relays regular copper unshielded cables were used. The connections are schematically displayed in Figure 3.10.

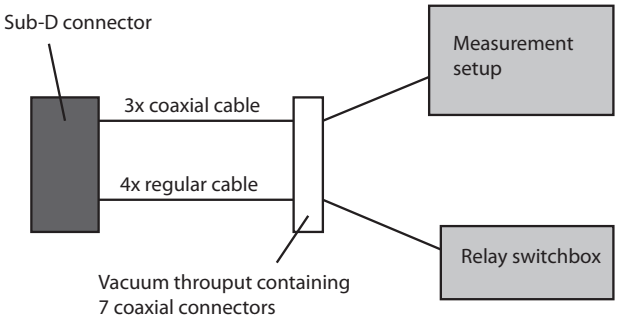

Figure 3.10: *Schematic representation of the connections established between the mini probe station and the measurement setup. It also shows the home built switch box used to switch the relays in the mini probestation*

A schematic picture of the electrical circuit in the mini probe station is depicted in Figure 3.11. On the bottom of the figure the four coaxial cables are shown. The three cables providing the connection with the measurement setup and a fourth coax EBIC cable which was connected to the SC detector inside the SEM. All the switches on the picture are in fact the relays controlled by connections in the sub-D connector going through the vacuum throughput as well. For clarity reasons these are left out of the drawing. Because the throughput only contains seven connectors, only 4 sets of relays could be controlled. Every relay in the picture is labeled with a letter, which indicate the set. Set C connects the measurement setup with the probe station. Both the SC detector as the measurement setup have their own ground. Having two different grounds can cause failure of the cell, so when the cell is connected to the SC detector the set of relays labeled A disconnects the measurement setup from the cell.

Set A and set B are used in RCI mode. A simplified schematic, where all the open connections are removed is depicted in Figure 3.12a. Here the relay set B is closed and set A is open. This way the "right" part of the PCM is connected to the ground and the "left" part is connected to the SC detector. Figure 3.12b shows the setup when relay set B is open and set A is closed. Now the "left" side of the PCM is connected to the ground while the "right" side is connected to the SC detector. This way the test nodes could be reversed without opening the SEM. The last relay D, provides a 330 kΩ series resistance. This resistance is needed to protect the cell against static discharges.

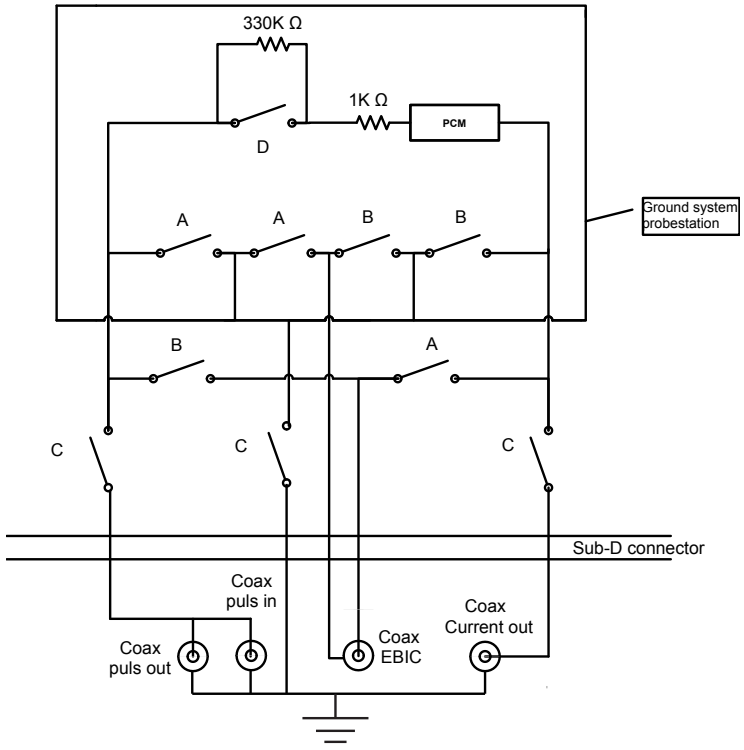

Figure 3.11: *Electric circuit of the mini-probestation*

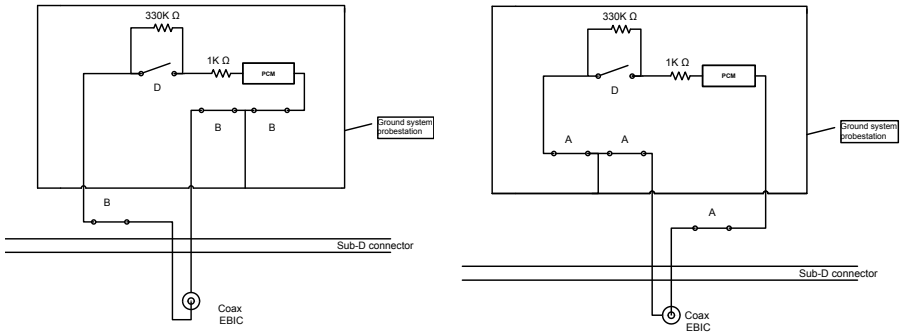

(a) (b)

Figure 3.12: *(a) Schematic circuit of the sample with left node connected to the SC detector and the right node to the ground.(b) Switching a relay set can reverse the connection. Now the left node is connected to the ground and the right node to the SC detector.*

Chapter 4

Results and Discussion

4.1 Result of the Bonded samples

As described in the previous chapter, the first tests were done by wire bonding the PRAM-cells and thus establish a connection with the SC detector. Figure 4.1a shows such a connection. A high contrast between the connected bond pads and the surrounding area can be observed. However as the image also indicates, a large acceleration voltage of 30kV is used to create such a contrast. Even though this high acceleration voltage is used, it was impossible to create a sufficient contrast to observe the PRAM cell itself with RCI. This is depicted in Figure 4.1b. This picture shows where the phase-change cell itself is located, however this can not be visualized even with these high acceleration voltages.

Figure 4.2a shows the a image of a sample treated with the 40% HF solution. As explained in the previous chapter the cell was over etched and the complete oxide layer was vanished away. However the picture shows a lot more contrast and more detail than Figure 4.1 even though this image is taken with a much lower acceleration voltages (3-5kV). Figure 4.2b shows a zoomed in image of one of the cells. Here a big contrast between the phase-change cell and its surrounding is observed. Interestingly though, this specific cell was not even connected to the SC detector. The reason a detailed image is still observed lies in the fact that the bonded wires also can pick up secondary electrons, scattered from the surface of the sample. It can be concluded from this that measuring in SC mode results in a combined image of secondary electrons from

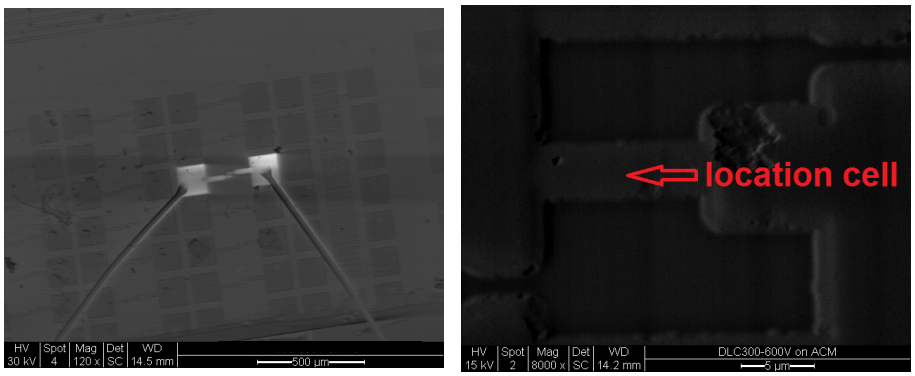

(a) (b)

Figure 4.1: *(a) RCI image of a PRAM cell connected with bonding wires. (b) Zoomed in RCI image. Although a high acceleration voltage is used, the phase-change cell is not visible.*

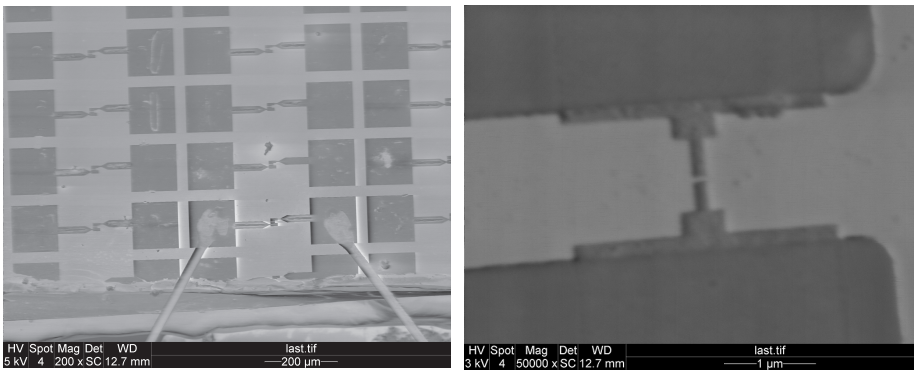

(a) (b)

Figure 4.2: *(a) Sample treated with 40% HF solution. The complete passivation layer is vanished. (b) Non connected cell in RCI mode, visible because of scattered secondary electrons picked up by the bonding wires.*

the surface with "deeper" electron passing through the phase-change material. Secondary electrons originate within a few nanometers from the sample surface and therefore SE collection is very topographic related. As the passivation layer is completely removed in Figure4.2 a strong variation in topography is left and this way the secondary electron collection is dominant. To minimize the amount of contrast created by the secondary electrons the surface (above the

area of interest) should be as flat as possible. However, as showed by the AFM measurements the imprint of the hard mask will always be on the surface and this imprint will be incorporated in the RCI image.

4.2 Voltage biased grid

To enhance the image quality a grid was placed above the sample. A positive bias to this grid by an external power supply creates an electric field which could pick up the SE electrons, and would draw electrons out of the passivation layer. Figure4.3a shows a RCI image without an external voltage bias. Figure 4.3b is taken with a 60V bias from the power supply. The figure shows that applying an electrical field does not increase the details on the images, but seems to affect only the contrast of the image. This may suggest that indeed the SE electrons are shielded by the grid. The contrast between the cell and the surrounding is not enhanced, so probably the grid does not has an affect on the electrons injected in the sample. It can be concluded that this method does not improves the image quality and is thus not further investigated.

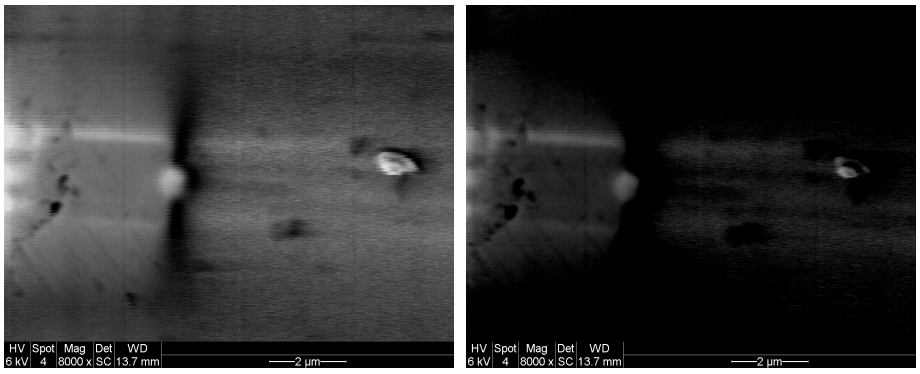

(a) (b)

Figure 4.3: *(a) RCI image of a cell. (b) Same image as (a) only now with a 60V bias. It does only seem to affect the contrast and does not enhance the image.*

4.3 Samples with FIB treatment

This section shows the results obtained with the samples treated by the FIB. Figure 4.4 shows three RCI images of a such a sample at different acceleration voltages. It can be seen that changing the acceleration voltage has dramatic effects on the quality of the obtained picture. Figure 4.4a shows the result with a low acceleration voltage. In this case the majority of the electrons do not have enough energy to reach the phase-change material, and thus a weak signal is detected by the SC detector. Figure 4.4b shows that a increase of the acceleration voltage result in more electrons with a penetration depth similar to the dept of the cell creating a higher resolution image. In the last image the acceleration voltage is too high. The majority of the electrons is this case will penetrate through phase-change material and therefore again can not be detected. Besides that it can been seen that Figure 4.4c is more "smeared out" than the previous two figures. The reason is that high energy electrons which hit the SiO_2 nearby the cell, have enough energy to reach the phase change material, and thus can be detected by the SC detector. Therefore it is very important always to optimize the acceleration voltage. Because these pictures are made before the mini-probestation was finished, this sample is connected the "old way", i.e. both nodes to the SC detector.

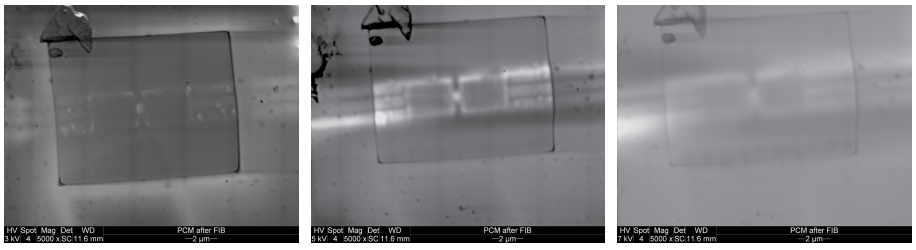

(a) (b) (c)

Figure 4.4: *(a) RCI image of a cell with a 3kV acceleration voltage. This appears to be too low for the electrons to reach the phase-change material.(b)Same cell with a 5kV acceleration voltage. (c)Same cell with 7kV acceleration voltage, which is too high.*

4.4 Result of the mini-probe station

4.4.1 Results of the samples milled by the FIB

AFM profile measurements show that the "hole" milled by the FIB above the cell used in Figure 4.4 is about 300 nm deep. A longer FIB treatment was used to create a deeper hole which could enhance the imaging quality. Because the cells are very sensitive to charging, bombarding them with high energy ions for a long time can easily result in destroying the cell. To reduce the charging effects in the SiO_2, and therefore catastrophic discharging through the phase-change cell, the organic conductive layer PEDOT:PSS was applied on top of this structures. This resulted in successfully creating samples whit a hole of about 800nm deep (measured with the AFM), without the cell being damaged. Figure 4.5 shows a SE image of such a cell. Because the passivation layer is reduced to only a few hundred nanometer, the phase-change cell is visible in SE mode. The dimensions of this cell are 700x380nm.

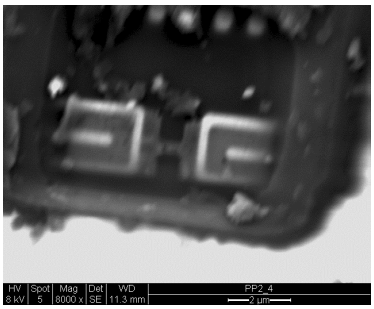

Figure 4.5: *SE image of a cell treated with the FIB. On the bottom of the hole the phase change is visible.*

Figure 4.6 shows two RCI images of the the same sample. The home built mini-probstation allows connecting one node of the cell to the ground and the other to the SC detector and even reverse these connections without opening the SEM. This results in a natural contrast around the amorphous mark as this is a barrier for the electrons. Electrons which hit the PCM on the side of the ground node will be drawn to the ground, while electrons which hit the PCM on the side of the SC detector have a bigger chance being measured by this detector. The resistance of the cell is measured in-situ so at all times the status of the cell is known. On Figure 4.6a the "left side of the cell" is connected

to the SC detector. Figure 4.6b shows the same cell with the ground and the EBIC connection reversed. Although the image does not have enough detail to precisely locate the amorphous mark, a clear contrast can been seen in the middle of the cell. Attempts to use Matlab to multiply the two images to make an estimation of the size of the amorphous mark have failed due to the low lateral resolution of the images.

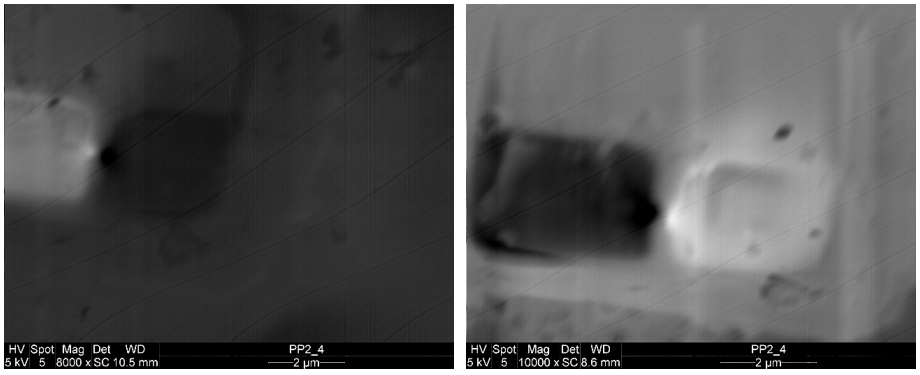

(a) (b)

Figure 4.6: *(a)RCI image of a cell with the left node connected to the SC detector and the right to the ground. A natural contrast can be seen in the middle of the cell.(b)Same cell with the reversed connections.*

The nature of the well defined contrast around the middle of the phase-change cells yet unknown. It suggest that a bigger number of electrons injected by the beam in this region reach the nodes (of either ground or SC detector). A possible explanation is a local internal field that push the electrons injected in the region towards either of the nodes. If the amorphous phase has a higher work function than crystalline phase electrons will flow from the amorphous region into the crystalline region to balance both the Fermi levels. Therefore the amorphous mark would have a slight positive charge (at the interface) creating an electrical field, referred to as the built-in potential. This built-in potential however is not yet confirmed for phase-change memory cells.

It should be noted that no pictures of the crystalline state could be obtained. Whenever the cell was switched to this state the SC image did not show any contrast because the whole cell is then grounded.

4.4.2 Results of the BHF etched samples

This section shows the results of the BHF etched sample (E6) for a cell with dimensions 2000x340nm. This cell is etched for 16 minutes and therefore the estimation of the amount of SiO_2 that is etched away is 800nm. Figure 4.7a shows an SE image of the cell with the plus and the minus sign labeling the anode and the cathode respectively. Figure 4.7b is an SC image of this cell in the crystalline state. This is remarkable as in the previous measurements there was no contrast at all in this state. The crystalline state was only visible in SC mode when it was connected to "ground A" and not with "ground B", assuming the series resistance is needed to create the contrast. The resistance of the cell in this state is measured to be 6 kΩ. The contours that define the contrast on Figure 4.7b are shown to have far bigger dimensions than Figure 4.7a. It can be concluded that not only electrons from the phase-change material are detected but maybe also electrons in the surrounding passivation layer and the secondary electrons scattered from the surface and detected by the needles. The latter can be seen by the bright line on the left of the contour. This is the side where the needles are located, so electrons on this side have a bigger chance of being detected. Calculations and Matlab filters are used to try to estimate the deviation in the SC images, but were without success. Because of a bad lateral resolution of the SC image, it appeared to be impossible to use them for these calculations.

After a RESET pulse was applied the cell was switched back to the amorphous state. Figure 4.8 shows this state. Even though the results of this sample were not sufficient to exactly distinguished the amorphous mark with its surrounding it did gave a better result than the sample with the FIB treatment showed in the previous section. A custom made Matlab filter was used to filter these images as there was a lot of noise (found to be 50 Hz noise), due to all the interference with electrical circuits from the mini-probe station.

Figure 4.8a shows the upper node connected to the SC detector and the bottom node connected to the ground. Figure 4.8b shows the connections reversed. In contrary to the crystalline state, only half the cell is visible in this state. The amorphous mark in the cell prevents electrons moving through the cell. Again the images do not have enough detail to allow any estimation about the size of the amorphous mark but it reveals roughly where it is located, i.e. on the side of the anode. This is in agreement with earlier findings showing the

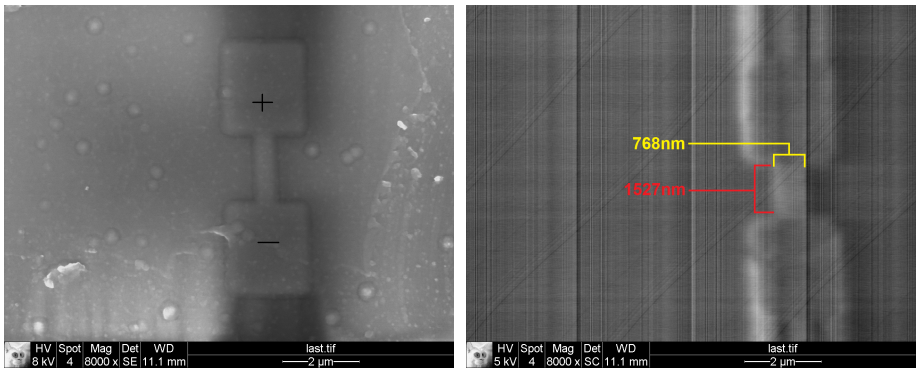

(a) (b)

Figure 4.7: *(a)SE image of a BHF etched sample (E6). The plus and minus depict the anode and cathode respectively.(b)SC image of the same cell in the crystalline state. The dimension of the picture are not in agreement with the dimensions of the PRAM cell.*

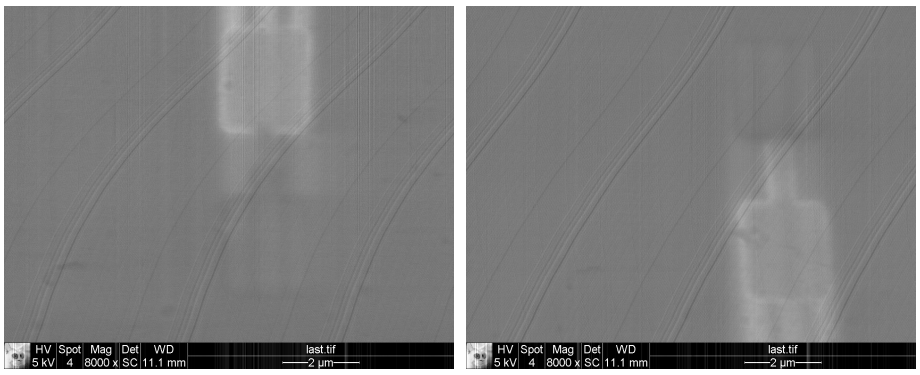

(a) (b)

Figure 4.8: *(a)RCI image of a cell with the "top" node connected to the SC detector and the "bottom" node to the ground. (b)Same cell with the reversed connections. The amorphous mark is located at the "top".*

Thomson effect in PRAM cells. This thermo-electric effect creates an asymmetry in temperature profile in the cell shifting the amorphous mark towards the anode [9]. The results of this study can be seen in Figure 4.9. This figure shows TEM images of of a phase-change cell. The amorphous mark can clearly be seen on one side of the cell i.e the side of the anode. When the cell is switched

with a reversed pulse direction the amorphous mark is shifted to the other side, towards the anode. Switching of this cell was not done *in-situ*.

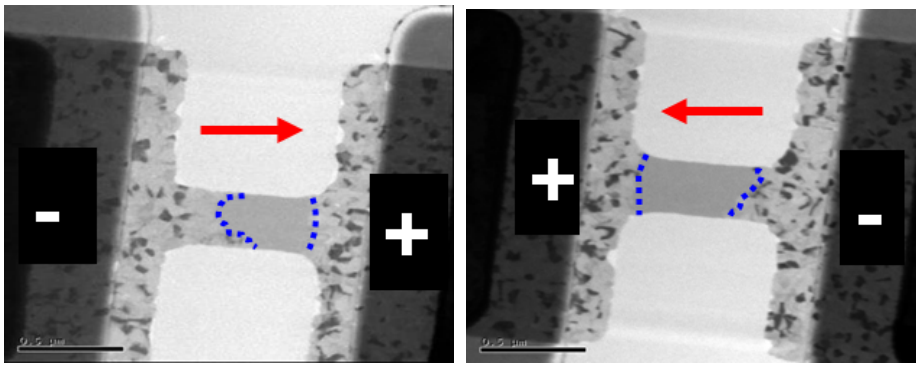

(a) (b)

Figure 4.9: *TEM images proving the Thomson effect in PRAM cell [9].*

The cell was switched back to the crystalline state by applying a SET pulse. This time however the direction of the pulse was reversed as can be seen on Figure 4.10a. The crystalline state is shown in Figure 4.10b. To see the influence of the Thomson effect the cell was switched to the amorphous state with a SET pulse in the direction as in Figure 4.10a. Figure 4.11 shows this for both nodes connected to the SC detector.

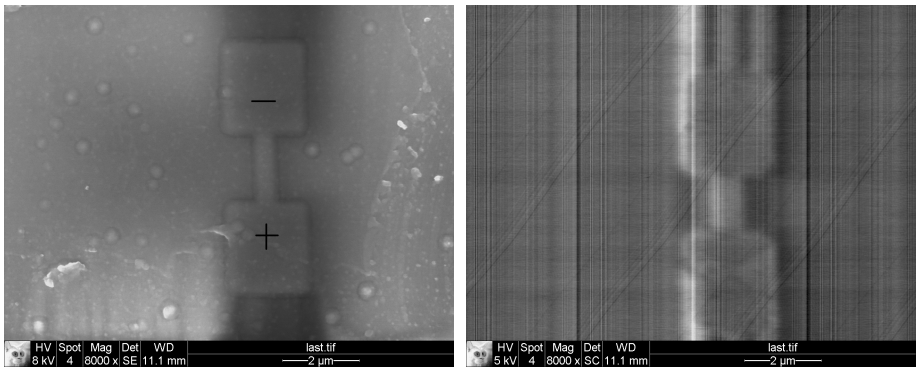

(a) (b)

Figure 4.10: *(a)SE image of a BHF etched sample (E6). The plus and minus depict the anode and cathode respectively.(b)SC image of the same cell in a crystalline state.*

It can been seen that the amorphous mark has shifted from the "top" of the cell to the center of the cell, towards the anode. Again the cell was crystallized and programmed into the amorphous state, again with the anode at the "bottom". Figure 4.12 shows this. Now the amorphous mark has completely shifted to the other side of the cell. This confirms the Thomson effect in the PRAM cells as described in [9].

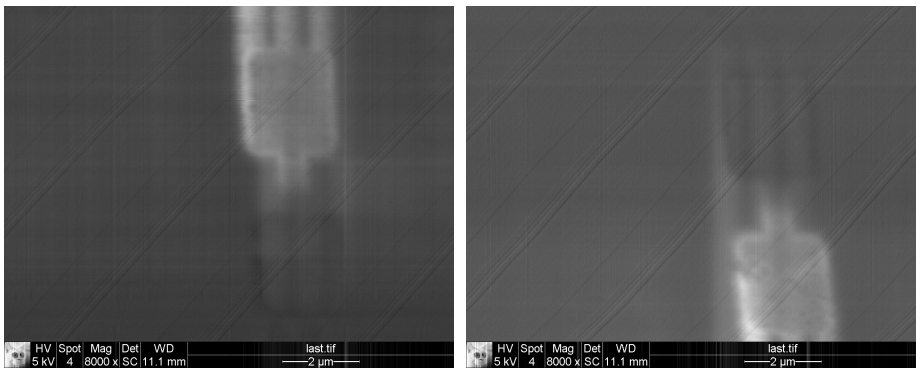

(a) (b)

Figure 4.11: *Sample E6 in the amorphous state. By reversing the pulse direction the amorphous mark has shifted towards the center.*

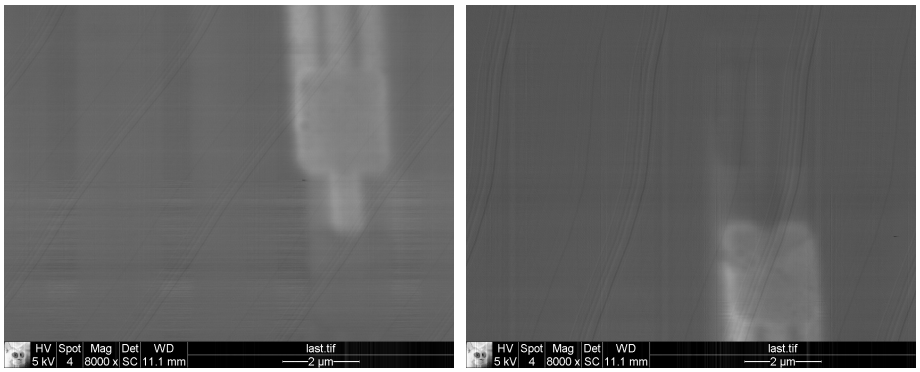

(a) (b)

Figure 4.12: *Sample E6 in the amorphous state. The amorphous mark has completely shifted to the other side of the cell.*

Chapter 5

Conclusions and Recommendations

It is possible to create a contrast with the EBIC detector in a PRAM cell, though the images did not show enough detail to exactly locate the amorphous mark. One of the main causes is the relative thick passivation layer on top of the PCM.

Two ways are tried to overcome this problem. Milling a hole in the passivation layer with the FIB just above the actual phase-change cell is drastically enhancing the RCI image. Though, due to the fact the cells are very sensitive to static discharges, the samples could easily be damaged so this process has to be done very carefully. To reduce the charging effect, and therefore the chance of damaging the cell, a conductive polymer PEDOT:PSS was spin coated onto the samples. This allowed making deeper holes with the FIB.

Another method to reduce the thickness of the passivation layer was etching with BHF. Because the passivation layer is composed of three different layers with unknown thickness only an estimation of the thickness reduction could be done. However by using different samples with different etching times switchable cells with a reduced amount of passivation layer could be created.

Although both methods resulted in better contrast and resolution, it still was not sufficient to "see" the amorphous mark.

A custom mini-probe station was successfully manufactured to examine the PRAM cells in the SEM. The relays allowed quick switching between the mea-

surement setup and the EBIC detector. By making use of the mini-probe station, *in-situ* switching of the PRAM cells between the crystalline and the amorphous state is realized in the SEM.

The Thomson effect in phase-change memory cells is verified. By reversing the pulse direction, a shift of the amorphous mark towards the anode was observed as described in [9]. In contrary to the previous study, this effect is observed *in-situ*.

It can be concluded that using CC microscopy does not provide an easy method for examining PRAM cells. To obtain a reasonable image a lot of effort has to put in removing the passivation layer and even then only a low resolution could be acquired. As preparing the samples is laborious it makes more sense to use the TEM to study these cells. This study has provided a good insight for achieving *in-situ* switchable cells in the TEM.

To obtain better results with CC microscopy in the SEM a better fine tuning of removing the passivation layer is needed. Also the connections should be further away from the cell, or preferable underneath the cell, so the secondary electrons cannot be detected.

Chapter 6

Acknowledgments

I first like to thank Jasper not only for his supervision through my entire research but also for teaching me all kind of stuff I did or did not want to know. His magical understanding of electrical circuits let me think he is the Harry Potter of micro electronics.

Bart, for his supervision and the fact I could always turn to him for questions.

I also want to thank Gert ten Brink for helping me making nice images and for making not so nice remarks. I also want to thank him for being in our group as otherwise I would be the heaviest Dutch guy.

My "roomies", Peter, Orcun and Gert for having the patience to answer all my questions about random stuff.

The rest of the group, George, Robin and Arno for the nice coffee breaks.

Bibliography

[1] Hudgens (2008), *Future of phase-change semiconductor memory devices*, Journal of Non-Crystalline Solids

[2] Welnic and Wuttig (2008), *Reversible switching in phase-change materials*, Materials Today, review article

[3] Wuttig (2005), *Towards a universal memory?*, Nature materials,

[4] Elfwing (2002), *Nanoscal Characterisation of Barries to Electron Conduction in ZnO Varsitor Materials*, Acta Universitatis Upsaliensis, Uppsala

[5] Leamy (1982), *Charge collection scanning electron microscopy*, Journal of Applied Physics, review article

[6] Smith (1986), *Resistive contrast imaging: A new SEM mode for failure analysis*, IEEE Transactions on electron devices

[7] Pandian (2008), *Phase-change thin films: resistance switching and isothermal crystallization studies*, Groningen University Press , Groningen

[8] Spierings (1993), *Wet chemical etching of silicate glasses in hydrofluoric acid based solutions*, Journal of Materials Science

[9] Castro (2009), *Evidence of the Thermo-Electric Thomson effect and Influence of the Program conditions and Cell optimization in Phase-Change Memory Cell*, IEDM